RSC Advances

ROYAL SOCIETY OF CHEMISTRY

www.rsc.org/advances

Silver/Gold Core/shell nanowire monolayer on a QCM microsensor for enhanced mercury detection

Paria Larki[1], Ylias M. Sabri[1], K. M. Mohibul Kabir[1], Ayman Nafady[2,3], Ahmad Esmaielzadeh Kandjani[1], Suresh Kumar Bhargava[1]**

[1] Centre for Advanced Materials and Industrial Chemistry (CAMIC), School of Applied Sciences, RMIT University, GPO Box 2476V, Melbourne, VIC 3001 (Australia).

[2] Department of Chemistry, Faculty of Science, Sohag University, Sohag, Egypt

[3] Department of Chemistry, College of Science, King Saud University, Riyadh, Saudi Arabia

*Email: ahmad.kandjani@rmit.edu.au, suresh.bhargava@rmit.edu.au, Phone:+61 3 99252330

KEYWORDS: Core/Shell, galvanic replacement, monolayer, Mercury sensing, gas sensing.

ABSTRACT

The formation of silver nanowire monolayer (Ag NWML) galvanically replaced with gold (Au) directly on the electrodes of a quartz crystal microbalance (QCM) transducer for non-spectroscopic based elemental mercury (Hg^0) vapor sensing is reported in this study. The modification of Ag NWML to Ag/Au alloyed (Ag/Au NWML) structures through galvanic replacement (GR) reaction was found to enhance the sensitivity and selectivity of the sensors. Following GR reaction, the morphology of the Ag nanowires was found to change without deforming the monolayer packing arrangement. Interestingly, the selectivity of the sensor toward Hg^0 vapor was increased by increasing the Au concentration during the GR reaction. The Ag/Au NWML based sensor which was modified using a 2 mM Au solution was found to produce 3 times higher sensitivity compared to the Au control QCM as well as having more than 95% accuracy and >90% repeatability. This was found to be due to the formation of Ag/Au alloys (Ag/Au NWML) with active sites that had high affinity toward Hg^0 vapor.

1. INTRODUCTION

The structural and morphological modifications of materials are the key in developing novel metallic materials with enhanced performances and engineered applications. The utilization of galvanic replacement (GR) reaction in metallic materials is one of the simplest and efficient methods used for developing alloyed and porous metallic nanostructures[1, 2]. This method among other modification methods (e.g. alloying/dealloying[3, 4] and core/shell methods[5, 6]) has attracted many researchers' attentions due to its highly tuneable and spontaneous nature. In addition to structural changes due to alloying, GR reaction can generate porous nanostructures[7]. Thus this method can provide highly active nanostructures

for applications such as catalysis and chemical sensing which require both high active surface area and selectivity toward a specific analyte[8, 9].

A classic example of GR reaction is the replacement of silver with gold which is usually carried out by immersing a silver based nanomaterial into a solution containing gold ions[10-12]. The type of alloy (i.e. Au content in Ag/Au alloy) and morphology will depend on the immersion time, gold ion concentration and solution temperature in which the Ag containing material is immersed. Ag nanowires with high aspect ratio have previously been used to form tubular Ag/Au alloy nanowires via galvanic replacement methods[13]. Although the synthesised nanowires reported had high aspect ratio with controlled porosity through GR reaction, they are not applicable to most device fabrication processes. This is because the synthesis procedures reported lack any control over the packing arrangement of the nanoparticles when deposited on the device surface. This is important as long range order and repeatable fabrication of the packing arrangement are required to attain high device performance for applications such as chemical sensing, optics and catalysis [14-16].

One of the well-known methods for depositing packed monolayer nanowires structures over large surface areas is the Langmuir–Blodgett technique [15, 17, 18]. Although this technique allows for the formation of uniform monolayer surfaces, it does however require specialised instrumentation and substrate surface modification (i.e. hydrophobic surfaces are required). Nevertheless when the Langmuir–Blodgett successfully produced monolayers of Ag nanowires and used for surface enhanced Raman spectroscopy (SERS) application, they showed considerable increase in the hot spot density on the substrate as a result of the packing arrangement and subsequently enhanced the detection limit of the SERS sensors[18]. In another packed assembly process presented by Yingpu Bi et al., silver nanowires were produced and repeatedly washed with water (three times in this case) over a nine hour period after which the nanowires were deposited at the bottom of the flask[19]. Although this process

proved to be straight forward, it did require lengthy procedures and was restricted by the requirement of polyol (PVP) being present in the solution and in controlled quantities.

A more promising method for forming packed assembly of nanoparticles is to use surfactants' affinity and repulsion toward other chemicals as a means of force to pack the monolayer together. The procedure is similar to the Langmuir–Blodgett technique in which the colloidal solution of the developed nanomaterial is transferred to the air/water interface before being packed and aligned through a shear force mechanically applied at the interface [14, 20]. The difference however lies in the method used to apply the force for the alignment of the materials to occur. In the Langmuir–Blodgett technique, the force is applied using the Langmuir trough to sweep the surface and bring the colloidal particles together. On the other hand, in the chemical method a monolayer of a surfactant is injected from one side of the interface and expands on the surface to form a monolayer which in the processes forces the colloidal particles to repel and move away to form packed, uniform and aligned monolayer. The formed colloidal monolayer can be picked up on the desired substrate or device. This fast and abrupt method only requires microliter (μl) amounts of nanoparticles and it is only dependent on the concentration of the materials.

One of the most dangerous heavy metal pollutants is elemental mercury (Hg^0) vapor as it can easily be transferred by air, convert to more toxic organic forms and accumulate in aquatic life forms thereby entering the food chain[21-24]. Small quantities of this toxin in the human body can produce several health problems, from neurotoxicity to even death[25, 26]. The main natural sources for this hazardous toxin are volcanic activities and bushfires. However, anthropogenic sources (i.e. coal-fired power plants, mining etc) make up more than half of the total global emissions, thereby making mercury emission reduction one of the top priorities for government and environment regulating bodies such as the United States environmental protection agency (US-EPA) and the United Nations' environmental

programme's (UNEP). This is of no surprise given the reports that in US alone, around 60,000 babies are born annually with diseases and symptoms related to mercury poisoning of their mother's placenta during pregnancy[27-30]. In order to reduce anthropogenic portion of the emissions, industries need to overcome several challenges in their mercury removal processes. The first and foremost step in this chain of processes is the sensing of toxic mercury which is mandatory both as a feedback system and as an assessment method to the mercury removal technology installed. The challenge comes from the conventional spectroscopy techniques for gas phase mercury sensing being highly expensive, not portable, requiring special sample pre-treatment and having low selectivity toward mercury when other harsh industrial gas species are present in the effluent[31]. These drawbacks have inspired the urge to develop alternative detection methods that are cheap, simple yet highly sensitive and selective toward Hg^0 vapor. In this work, we report on the fabrication of packed colloidal monolayer of Ag/Au nanowires deposited on quartz crystal microbalance (QCM) for selectively detecting low concentrations of Hg^0 vapor from simulated industrial gas effluents. The selectivity of the produced sensor was enhanced by controlling the Au content in the alloy through changing the conditions of the galvanic replacement reaction when forming the Ag/Au alloy structures. The results showed that by using nanowires with highly active surfaces as a result of the GR reaction, a robust, cheap, selective and sensitive sensor can be fabricated, which can potentially operate as an online Hg^0 vapor sensor as a substitute for the conventional spectroscopy techniques currently used by industry.

2. EXPERIMENTAL

2.1. Chemicals and materials

All chemicals used in this study were analytical grade and used as received. AT-cut quartz crystal substrates (10 MHz, optically polished and ⌀ 7.5 mm,) were ordered from AATA,

Japan. The quartz crystal microbalances (QCMs) were fabricated by evaporating (e-beam evaporation) 150 nm Ti on both sides of the quartz substrates as the QCM electrodes (⌀ 4.5 mm). According to Sauerbrey's equation, any change in the mass of the QCM electrodes induces a change in the resonant frequency of the transducer[32]. The resonant frequency of the fabricated QCM transducers were monitored by utilizing two saparate research quartz crystal microbalance (RQCM, Maxtek) units, each measuring the resonant frequency of two QCMs at a time with a resolution of ±0.03 Hz, thereby a total of for four QCMs were able to be tested at any one time.

2.2. Preparation of Ag nanowires

Ag nanowires were synthesized via the polyol method[33]. First, a 6 ml ethylene glycol solution containing 100 mM silver nitrate with 130 mM PVP (M_W~29k) were added to 6 ml ethylene glycol solution containing 80 µM Iron (III) chloride, both solutions being pre-heated to 150°C. Following a reaction period of 90 mins, the reaction was halted and the solution was left to cool down to room temperature. The produced Ag nanowires were centrifuged at 2000 rpm and washed three times with acetone and water.

2.3. Packing of nanoparticles with water/air interface

The preparation method for fabricating Ag/Au alloy nanowire monolayer (NWML) based QCM sensors are shown schematically in **Figure 1**. The prepared Ag material was diluted 10 times in ethanol. About 25 µl of the diluted solution was introduced through drop-wise addition on the water/air interface (**Figure 1a**), all in a glass petri dish ($⌀_i$ 10 cm containing 80%v/v water). The introduction of Ag nanowire solution was stopped when a thin layer of Ag nanowires was observed to have formed on about 2/3 of the water surface (**Figure 1b**). In order to pack the freely floating silver nanowires, ~10 µl of sodium dodecyl sulphate (SDS) 20 wt% aqueous solution was added (drop-wise) from the edge of the petri dish (**Figure 1c**)

thereby forcing the Ag nanowires to pack together on one side of the (**Figure 1d**). The formed silver monolayer was transferred onto the Ti-QCM (**Figure 1e**) by simply dipping the QCM into the petridish and removing it over a 30s period, followed by drying under N_2 atmosphere.

2.4. Galvanic replacement of Ag nanowires with gold

The GR reaction was carried out by immersing the silver nanowires monolayer pre-deposited on the QCMs into a $HAuCl_4$ aqueous solution with a range of different concentrations (0.05, 0.1, 0.5, 1 and 2 mM) at 25°C with each substrate being left in their respective solutions for a period of 2 min (**Figure 1f**). A higher Au concentration (>2 mM) was found to fail the sensor fabrication process due to the formation of thick layers of the alloy which resulted in the sensitive layer being peeled off the surface of the QCM electrodes. In order to remove the $AgCl_2$ salt that is formed on the surface during the GR reaction, the QCMs were dipped into a 25% ammonia solution to dissolve the salt. The QCMs were finally washed with water and dried using dry nitrogen.

2.5. *Mercury vapor sensing*

The QCMs tested in this study were ensured to have high quality (Q-factors >3000) as was required by the in-house built calibration system, calculated using the method reported previously[34]. The developed QCM sensors' performance were tested toward elemental mercury vapor sensing in a dynamic range of Hg^0 vapor concentrations at two operating temperatures of 30°C and 75°C ± 1°C. The operating temperatures were selected based on their relevance to room temperature sensing and on-field sampling conditions used by industry to sample Hg^0 vapor[35]. In addition, the selectivity of the sensors toward Hg^0 vapor were tested by exposing the sensors toward Hg^0 vapor in the presence of industrial simulated effluent gases containing ammonia, (NH_3, 384 ppm), ethyl mercaptan (Ethyl-M, 2.61 ppm),

acetaldehyde (Ac-ald, 304 ppm), dimethyl disulfide (DMDS, 5.01 ppm), methyl ethyl ketone (MEK, 40.1 ppm) and high levels of humidity (H_2O, 27.2 g/m^3). These gases were selected as they have high affinity toward gold and/or exist in most industrial stack effluents. NIST certified elemental mercury permeation tubes (VICI, USA) were used for the generation of different concentrations of Hg^0 vapor. The permeation tubes were validated using $KMnO_4$ impinger train calibration system (modified version of Ontario-Hydro method) and employing Agilent 7700 series inductively coupled plasma mass spectroscopy (ICP-MS, ShieldTorch system) for their analysis. The custom designed gas sensor cell enabled the testing of four QCMs at the same time where a continuous test pattern was undertaken over a 25 day period. A sensing event consisted of the QCMs first being exposed to dry N_2 gas stream which had a known concentration of Hg^0 vapor with/without the presence of other interferent gases for a period of 1 h. This step was then followed by the QCMs being exposed to dry N_2 gas stream for another 1 h period. The total gas flow rate was maintained constant at 200 sccm throughout both steps of each 2 h sensing event by utilizing mass flow controllers purchased from MKS instruments, USA.

3. RESULTS AND DISCUSSION

The SEM images of Ag NWML with two different magnifications are shown in **Figures 2a** and **2b**. The synthesised Ag nanowires were observed to have 3 µm length and 70 nm average size with smooth surface. The SEM image obtained at low magnification (**Figure 2a**) shows a packed monolayer of Ag nanowires. The packing faults observed in the SEM images is due to the differences in size distribution and drying effects during monolayer formation process[36, 37], and has been reported numerous times for systems where different types of nanoparticles are used to form packed monolayers[18, 38]. Even so, the subsequent packing configuration of the monolayers formed on the different QCM substrates were observed to be consistent, thereby the QCM devices are expected to produce similar sensing characteristics.

Furthermore the current monolayer formation technique is reliable in achieving repeatable packed monolayer configuration with similar packing faults compared to other common particle assembly techniques, most of which are disadvantaged by random agglomeration between different samples[15-18, 39, 40].

The GR reaction of the Ag-NWML with Au was found to form small Au nanoparticle deposits on the surface. Increasing the concentration of the Au solution was found to increase the size and the coverage of Au on the Ag-NWML (**Figure 2d-e**). The morphology of the Ag-NWML were found to change drastically by increasing the Au concentration when performing GR reaction, converting from semi-spherical nanoparticles at low concentrations to nano-flower like morphologies at relatively higher concentrations. The SEM images (**Figure 2h**) also confirmed that the packing arrangement of the monolayer does not change following the GR reaction and ammonia washing processes, even when the highest Au concentration of 2 mM was used in the reaction. The TEM images shown in **Figure 3** were obtained in order to understand the uniformity of the Au nanostructures on individual alloy nanowires (Ag/Au-NWML) formed through GR reaction. The Ag-NWML in **Figure 3a** is observed to have a relatively smooth surface compared to the galvanically replaced Ag/Au-NWML. These microscope images indicate that the detachment of Ag atoms and their replacement with Au changes both surface roughness and morphology of the Ag-NWML. The TEM images also show that the size of the Au nanostructures increased with increasing Au concentration. The major advantage of using Ag-NWML instead of optically polished substrates when undergoing GR reactions on a sensing layer is that the NWML structures produce a more uniform Au structure formation (**Figures 2** and **3**) relative to the optically polished surfaces presented in our previous publications[9, 31]. The more uniform deposits of Au nanostructures on the Ag-NWML relative to optically polished substrates is due to GR reaction preferably occurring on the high energy, defected areas of the nanowires which are

otherwise expected to be scarce and random on polished substrates. The newly formed surface defects as a result of GR reaction have been shown to have tremendous role in applications like electrocatalysis and sensing[14, 41, 42].

The crystal structure and surface composition studies of the galvanically replaced samples were carried out using XRD and XPS techniques, respectively. **Figure 4a** shows the XRD pattern of Ag-NWML and Ag/Au-NWML where the peaks in Ag-NWML correlated well with the (111), (200), (220) and (311) planes of the Ag structure (JCPDF 65-8428). The XRD patterns of the samples before and after GR reaction are similar and no other crystalline impurities are observed in the pattern. As both gold and silver have face centre cubic (FCC) structure with similar lattice parameters, they have similar XRD patterns. Thus, the formation of Ag/Au nanoparticles on the silver structure would not generate a secondary pattern in the structure. However, a higher resolution XRD characterisation on (111) plane in **Figure 4b** revealed that the peak position changed following GR reaction. The formation of Ag/Au alloy after GR reaction can be confirmed by considering the phenomenon of shifting of the XRD pattern that occur toward lower 2θ vales[9]. To validate the formation of metallic Au on Ag-NWML, the highly sensitive surface spectroscopy technique, namely XPS studies, were carried out before and after the GR reaction. **Figure 5a** shows the XPS survey spectra for Ag-NWML and Ag/Au-NWML before and after GR (Au 1mM) where the Au core level peaks in the survey spectra show the formation of the gold structures on the Ag-NWML. **Figure 5b** shows that the Ag $3d_{3/5}$ core level of Ag-NWML appeared at 368.2 eV thereby confirming the existence of elemental silver[43]. The Au ions are expected to replace the Ag atoms in the GR reaction due to the difference in the electrochemical potentials of the two half reactions (i.e. $AuCl_4^- + 3e \rightarrow Au^0 + 4Cl^-$ (+0.93V) and $Ag^+ + e \rightarrow Ag^0$ (+0.7996V) vs. H_2 standard electrode). The Au deposited on the Au-NWML was found to be in the elemental form due to the appearance of the Au $4f_{7/2}$ at 84.2 eV[10, 42]. XPS analysis can only provide

characterisation information from the top few nanometers of the surface, thereby making it a highly sensitive spectroscopy technique for surface studies. On the other hand, EDX has a depth of field of few micrometers and so can be used to obtain an overall understanding of the sample composition at greater depths. Thus, EDX analysis were carried out to study the atomic portion of the structure related to the developed NWML directly on QCM devices using GR reaction (**Figure 6**). The formation of Au on Ag nanowires was also confirmed through the analysis of their EDX spectra, before and after the GR reaction. The gold content in each sample (Au/(Au+Ag)) was deduced from the EDX spectra, showing that the Au content increased with increasing Au concentration used when undergoing GR reaction. The Au content was observed to increase drastically when a 2 mM gold solution was used where most of the alloy structure was composed of gold rather than silver.

3.2. Mercury sensing results

Mercury vapor sensing experiments were carried out at 30ºC for all QCM sensors (Au-control and galvanically replaced Ag/Au alloy samples). The sensors were exposed toward Hg^0 vapor concentrations of 0.31, 0.45, 0.64, 0.93, 1.27, 1.74, 2.38 and 3.26 ± 0.05 mg/m^3 sequentially, from lowest to highest concentrations. The dynamic responses of the sensors are shown in **Figures 7a** and **7b**. The response magnitude of Au-control is observed to be higher than the QCMs galvanically replaced with 0.05 mM (Ag/Au 0.05 mM) and 0.1 mM (Ag/Au 0.1 mM) Au possible due to the relatively low gold nanostructure content deposited on their surfaces. Interestingly, by increasing the Au concentration in GR reaction to 0.5 mM the developed QCM (Ag/Au 0.5 mM) showed a significant enhancement in response magnitude when compared to the Au-control based QCM. This indicated that high sensitivities of the developed sensors can be controlled by changing the Au concentrations during GR reaction, where small increase in Au contents can significantly increase the surface affinity toward Hg^0 vapor. It can be observed from **Figure 7b** that the

response magnitudes of the sensors increased further when Ag/Au 1 mM and Ag/Au 2 mM were tested. The later, highly sensitive QCM based Hg^0 vapor sensors developed were further tested at an operating temperature of 75ºC. It can be observed from **Figure 7b** that the response magnitudes of both QCM sensors (1 and 2mM Ag/Au) slightly decreased when the operating temperature was elevated from 30 to 75°C. It is well known that the vapor pressure of Hg^0 increases at the higher operating temperatures thereby reducing the tendency of mercury vapor atoms to undergo sorption processes on the solid QCM surfaces and so a decrease in the device sensitivity is observed[14]. On the other hand, at relatively higher temperatures, Hg^0 desorption (sensor recovery step of the sensing event) from the surface can be enhanced thereby decreasing the sensor drift that results mercury accumulation[14]. Corresponding calibration curves for all the QCM sensors that were tested are shown in **Figures 7c** and **7d**. The sensors' trends in the Hg^0 sensing performance can be better analysed from these calibration curves. The Ag/Au 2 mM showed ~3 times higher response magnitude relative to the Au-control when tested toward 3.26 mg/m^3 of Hg^0 vapor. This increase is not only due to the alloy formed following GR reaction but also due to the drastic morphology changes that had occurred as a result of the reaction thereby increasing the surface area and active sites that have high affinity toward Hg^0 vapor. The effect of active sites (sharp edges and surface defects) on enhancing the electrochemical and sensing performances of the sensors has been reported in previous work[22]. In particular, Hg^0 vapor has been shown to have high affinity toward surface defect sites on Au substrates[44]. It has also been reported that GR reactions can produce nanostructures with relatively higher surface area as the formation of noble metal on the sacrificing underlying metal structure yields hollow morphologies. Therefore it is postulated that the galvanically replaced substrates occupy high surface area, not only due to the formation of flake and particle like shapes but also due to the formation of hollow structures at high Au concentrations. The high

surface area and formation of surface defects that are active toward Hg^0 vapor are thought to be the reason for the high affinity of the Ag/Au-NWML toward Hg^0 vapor during the sensing experiments. That is, Ag was employed as a highly sensitive material toward Hg^0 vapour while it has been reported to have low selectivity toward the toxin (ACS.App.Mat) . Au on the other hand was used to introduce the high selectivity and at the same time, by undergoing alloyed Ag/Au nanostructure formation through GR reaction, the sensitivity as well as sensitivity were observed to enhance. This is postulated to be due to the formation of defect sites on the alloy structure thereby producing sorption sites with high affinity toward Hg^0 vapor.

The statistical analysis of the sensors' performances is listed in **Table 1**. The method used to calculate the limit of detection (LoDs) of the sensors was based on determining the 3 standard deviation of the blank sample (no Hg^0 exposure) over a 1 h testing period. It was found that the LoD of the QCM sensors were significantly lower for the devices that were modified with a relatively high Au concentration. It can be observed from **Table 1** that the LoD of the Ag/Au 1 mM and Ag/Au 2 mM sensors at 30°C were 48 and 39 $\mu g/m^3$, respectively. In comparison, the LoD of the Au-control was found to be more than double the magnitude at 116 $\mu g/m^3$. The LoD of the Ag/Au 1 mM and Ag/Au 2 mM sensors were found to increase to 65 and 53 $\mu g/m^3$, respectively, at the elevated operating temperature of 75°C thereby indicating that the LoD of the sensors are deteriorated with increasing temperatures. It is noteworthy that galvanically replaced sensors can be utilized to operate at high operating temperatures while detecting low concentrations of Hg^0 vapor as is required by many Hg^0 emitting industries.

The sensors were tested towards detecting 3.26 mg/m^3 of Hg^0 vapor in 6 consecutive sensing events in order to calculate their repeatability and accuracy. The repeatability of the sensors were determined by calculating their coefficient of variance (CoV) which is a well-known

and accepted method for determining sensor repeatability[31]. The accuracy of the sensors were calculated while maintaining a contingency of ±10%[22]. As stated in **Table 1**, the repeatability of all sensors tested were around 90%, which is excellent when compared to the Au-control counterpart. It can also be observed from **Table 1** that the accuracy of the sensors while detecting Hg^0 vapor significantly increased with the Au concentration used during GR reaction. As shown, an accuracy of $\geq$ 99% (±10% contingency) was achieved for the Ag/Au 2 mM QCM at both operating temperatures, which is well above the 66.67% value observed for the Au-control QCM at 30°C. The accuracy of the 1mM QCM is lower than that of the 2mM at each operating temperature. The reduced accuracy observed for the 1mM QCM (shown in **Table 1**) is postulated to be due to the QCM having a higher noise profile observed in **Figure 7b** possibly reducing from a lower quality (Q-factor).

The sensors were exposed towards Hg^0 vapor concentration of 3.26 mg/m^3 in the presence of six common industrial interferent gases including ammonia, acetaldehyde, ethyl mercaptan, dimethyl disulfide, methyl ethyl ketone, and high levels of humidity in order to determine the selectivity of the sensors towards low concentrations of Hg^0 vapor. **Figures 8a** and **8b** show the selectivity of all sensors at the operating temperature of 30 and 75°C, respectively. As shown in **Figure 8a**, except for the presence of humidity, the Hg^0 vapor concentrations reported by the sensors did not vary significantly from the actual exposed concentration (red lines in the **Figure 8**) when either of the other interfering gas species or their combination was present with Hg^0 vapor. That is, the introduction of high levels of humidity tested was observed to significantly decrease the selectivity of the sensors at 30°C thereby resulting in the sensors reporting a much higher Hg^0 vapor concentration than that actually present in the vapor. As the devices used in this study are based on mass changes (i.e. QCM), the low operating temperature of 30°C is thought to promote the condensation of the high humidity content on the QCM surface thereby the sensor reports a response magnitude related to both

humidity and mercury sorption on the surface. This postulation was confirmed when the cross-interference related to humidity was observed to reduce at the elevated operating temperature of 75°C (**Figure 8b**) due to the tendency of the water molecules to stay in the gas phase rather than condense on the sensor surface. The water molecules tendency to stay in air even though the humidity content remained the same as that at 30°C, is due to the relative humidity being significantly reduced at 75°C (~90% RH at 30°C vs ~11% RH at 75°C). It can also be observed from **Figure 8a** that the increase in Au concentration during GR reaction significantly increased the selectivity of the sensors where the Ag/Au 2 mM sensor showed the highest selectivity. This indicates that the developed sensors can potentially be used as Hg^0 vapor detectors in industrial processes.

4. CONCLUSION

In summary, in this paper we have demonstrated a facile method for producing Ag/Au alloy nanowire packed monolayer based sensor devices. The monolayer formation was carried out using air/water interface method for Ag nanowires and the packed Ag nanowire monolayers were then transferred on to the surface of QCM electrodes. Different structures and compositions of Ag/Au alloys were synthesized by controlling the Au concentration used during galvanic replacement (GR) reaction of Ag NWML with Au salt. The results showed that by increasing the Au concentration during the GR reaction, the smooth surfaces of silver nanowires changed into more porous nanostructures of Ag/Au alloy nanowires. The produced QCMs were tested for detecting mercury vapor in the presence of simulated industrial effluents which included gas species such as ammonia, ethylmercaptan and high levels of humidity ($27.2 g/m^3$) just to name a few. It was found that the morphological changes that occur during GR reaction due to increased Au content in the Ag/Au alloy structures enhances the sensitivity and selectivity of the developed sensors toward Hg^0 vapor. The developed

sensors operate well at 75°C making them relevant to potentially detecting mercury from industrial gas effluents.

ACKNOWLEDGEMENTS

Authors acknowledge the RMIT microscopy and microanalysis facility (RMMF) for allowing the use of their comprehensive facilities and services. A.N. and S.K.B. would like to thank Deanship for Scientific Research, Visiting Professor Program at King Saud University, for partial support of this work.

SUPPORTING INFORMATION AVAILABLE

No supporting information

COMPETING FINANCIAL INTEREST:

The authors declare no competing financial interests

REFERENCES

1. C. M. Cobley and Y. Xia, *Mater. Sci. Eng. R-Rep.*, 2010, **70**, 44-62.
2. M. A. Mahmoud, R. Narayanan and M. A. El-Sayed, *Acc. Chem. Res.*, 2013, **46**, 1795-1805.
3. J. Erlebacher, M. J. Aziz, A. Karma, N. Dimitrov and K. Sieradzki, *Nature*, 2001, **410**, 450-453.
4. W.-S. Chae, D. V. Gough, S.-K. Ham, D. B. Robinson and P. V. Braun, *ACS Appl. Mater. Inter.*, 2012, **4**, 3973-3979.
5. C. N. Brodsky, A. P. Young, K. C. Ng, C.-H. Kuo and C.-K. Tsung, *ACS Nano*, 2014, **8**, 9368-9378.
6. R. Ghosh Chaudhuri and S. Paria, *Chem. Rev.*, 2011, **112**, 2373-2433.
7. V. Bansal, H. Jani, J. Du Plessis, P. J. Coloe and S. K. Bhargava, *Adv. Mater.*, 2008, **20**, 717-723.
8. A. P. O'Mullane, *Nanoscale*, 2014, **6**, 4012-4026.
9. B. Lay, Y. M. Sabri, S. J. Ippolito and S. K. Bhargava, *Phys. Chem. Chem. Phys.*, 2014, **16**, 19522-19529.
10. S. V. Jenkins, T. D. Gohman, E. K. Miller and J. Chen, *J. Chem. Educ.*, 2015, **92**, 1056-1060.
11. J. Chen, J. M. McLellan, A. Siekkinen, Y. Xiong, Z.-Y. Li and Y. Xia, *J. Am. Chem. Soc.*, 2006, **128**, 14776-14777.
12. S. E. Skrabalak, J. Chen, Y. Sun, X. Lu, L. Au, C. M. Cobley and Y. Xia, *Acc. Chem. Res.*, 2008, **41**, 1587-1595.
13. Y. Sun and Y. Xia, *J. Am. Chem. Soc.*, 2004, **126**, 3892-3901.
14. Y. M. Sabri, A. E. Kandjani, S. J. Ippolito and S. K. Bhargava, *ACS Appl. Mater. Inter.*, 2015, **7**, 1419-1499.
15. A. R. Tao, J. Huang and P. Yang, *Acc. Chem. Res.*, 2008, **41**, 1662-1673.
16. J.-W. Liu, H.-W. Liang and S.-H. Yu, *Chem. Rev.*, 2012, **112**, 4770-4799.
17. P. Yang and F. Kim, *ChemPhysChem*, 2002, **3**, 503-506.
18. A. Tao, F. Kim, C. Hess, J. Goldberger, R. He, Y. Sun, Y. Xia and P. Yang, *Nano Lett.*, 2003, **3**, 1229-1233.
19. Y. Bi, H. Hu and G. Lu, *Chem. Commun.*, 2010, **46**, 598-600.
20. J. R. Oh, J. H. Moon, S. Yoon, C. R. Park and Y. R. Do, *J. Mater. Chem.*, 2011, **21**, 14167-14172.
21. A. E. Kandjani, Y. M. Sabri, M. Mohammad-Taheri, V. Bansal and S. K. Bhargava, *Environ. Sci. Technol.*, 2015, **49**, 1578-1584.
22. Y. M. Sabri, S. J. Ippolito, J. Tardio, V. Bansal, A. P. O'Mullane and S. K. Bhargava, *Sci. Rep.*, 2014, **4**.
23. J. M. Cossaboon, P. M. Ganguli and A. R. Flegal, *Proc. Natl. Acad. Sci. U.S.A.*, 2015, DOI: 10.1073/pnas.1506520112.
24. C. A. Choy, B. N. Popp, J. J. Kaneko and J. C. Drazen, *Proc. Natl. Acad. Sci. U.S.A.*, 2009, **106**, 13865-13869.
25. L. Magos and T. W. Clarkson, *Ann. Clin. Biochem.*, 2006, **43**, 257-268.
26. T. Syversen and P. Kaur, *J. Trace Elem. Med Biol.*, 2012, **26**, 215-226.
27. J. Qiu, *Nature*, 2013, **493**, 144-145.
28. P. W. Davidson, G. J. Myers and B. Weiss, *Pediatrics*, 2004, **113**, 1023-1029.
29. M. Gilbertson and D. O. Carpenter, *Environ. Res.*, 2004, **95**, 240-246.
30. D. G. Streets, M. K. Devane, Z. Lu, T. C. Bond, E. M. Sunderland and D. J. Jacob, *Environ. Sci. Technol.*, 2011, **45**, 10485-10491.

31. Y. M. Sabri, S. J. Ippolito, A. J. Atanacio, V. Bansal and S. K. Bhargava, *J. Mater. Chem.*, 2012, **22**, 21395-21404.
32. G. Sauerbrey, *Zeitschrift für Physik*, 1959, **155**, 206-222.
33. Y. Sun, B. Gates, B. Mayers and Y. Xia, *Nano Lett.*, 2002, **2**, 165-168.
34. Y. M. Sabri, S. J. Ippolito, M. Al Kobaisi, M. J. Griffin, D. R. Nelson and S. K. Bhargava, *J. Mater. Chem.*, 2012, **22**, 20929-20935.
35. M. Levlin, E. Ikävalko and T. Laitinen, *Fresenius J. Anal. Chem.*, 1999, **365**, 577-586.
36. O. D. Velev and S. Gupta, *Adv. Mater.*, 2009, **21**, 1897-1905.
37. F. Li, D. P. Josephson and A. Stein, *Angew. Chem. Int. Ed.*, 2011, **50**, 360-388.
38. A. Tao, P. Sinsermsuksakul and P. Yang, *Nat Nano*, 2007, **2**, 435-440.
39. S. Acharya, J. P. Hill and K. Ariga, *Adv. Mater.*, 2009, **21**, 2959-2981.
40. H. Cong, B. Yu, J. Tang, Z. Li and X. Liu, *Chem. Soc. Rev.*, 2013, **42**, 7774-7800.
41. B. J. Plowman, M. R. Field, S. K. Bhargava and A. P. O'Mullane, *ChemElectroChem*, 2014, **1**, 76-82.
42. C. Liusman, S. Li, X. Chen, W. Wei, H. Zhang, G. C. Schatz, F. Boey and C. A. Mirkin, *ACS Nano*, 2010, **4**, 7676-7682.
43. A. E. Kandjani, M. Mohammadtaheri, A. Thakkar, S. K. Bhargava and V. Bansal, *J. Colloid Interface Sci.*, 2014, **436**, 251-257.
44. M. A. George and W. S. Glaunsinger, *Thin Solid Films*, 1994, **245**, 215-224.

Table captions

Table 1 Sensors' performance when tested toward Hg^0 vapor concentration of 3.26 mg/m^3 at 30°C and 75°C. The parameters calculated include limit of detection (LoD), accuracy and repeatability.

Figure captions

Figure 1 Schematic fabrication process for Ag/Au alloy nanowire monolayer (NWML) based QCM sensors, **a)** gradual addition ethanolic colloidal solution of Ag nanowires to the Water/Air interface; **b)** formation of unpacked Ag nanowires at the water/air interface; **c)** addition of SDS surfactant from the edge of the petri-dish; **d)** formation of packed Ag NWML due to the SDS molecules forming a monolayer on the water surface; **e)** transfer of the formed Ag NWML on to the Ti-QCM electrode surface; **f)** dipping of the formed AgNWML into Au solution with different concentrations to form Ag/Au alloy NWML through GR reaction directly on the sensors.

Figure 2 SEM images of **a)** Ag NWML, low magnification and **b)** high magnification, **c)** Ag/Au NWML (Au 0.05 mM), **d)** Ag/Au NWML (Au 0.1 mM), **e)** Ag/Au NWML (Au 0.5 mM), **f)** Ag/Au NWML (Au 1 mM) **g)** Ag/Au NWML (Au 2 mM), high magnification and **h)** Ag/Au NWML (Au 2 mM), low magnification.

Figure 3 TEM images of **a)** Ag, **b)** Ag/Au 0.05 mM, **c)** Ag/Au 0.1 mM, **d)** Ag/Au 0.5 mM, **e)** Ag/Au 1 mM, **f)** Ag/Au 2 mM nanowires.

Figure 4 a) XRD pattern of Ag/Au alloy monolayers and **b)** high resolution XRD pattern for Ag (111) peak showing shifting in the XRD with increased Au concentration during GR reaction.

Figure 5 a) XPS survey spectra for Ag- NWML and Ag/Au-NWML before and after GR reaction (Ag/Au 1 mM); **b)** Ag 3d and **c)** Au 4f core level spectra for Ag/Au-NWML (Ag/Au 1 mM).

Figure 6 a) EDX spectra of Ag and Ag/Au NWMLs (Au 2 mM) and **b)** atomic ratio Au/(Au+Ag) vs. Au concentration used in the GR reaction.

Figure 7 Hg sensing performance of the developed QCM sensors showing **a)** dynamic responses and b) response magnitude at 30°C for Au-control and Au/Ag NWML (Au=0.05 ,0.1, 0.5 mM) and **a)** dynamic responses and b) response magnitude at 30 and 75°C for Au/Ag NWML (Au=1 and 2 mM)

Figure 8 Selectivity performance of QCM based sensors toward Hg^0 vapor at **a)** 30 ºC and **b)** comparison of 30 and 75°C. The solid red lines in each graph represent the tested Hg^0 vapor concentration of 3.26 mg/m^3.

Tables

Table 1

	30ºC						75ºC	
	Au-Ctrl	0.05mM Ag/Au	0.1mM Ag/Au	0.5mM Ag/Au	1mM Ag/Au	2mM Ag/Au	1mM Ag/Au	2mM Ag/Au
LoD ($\mu g/m^3$)	116	302	129	53	48	39	65	53
Accuracy (%)	66.67	66.67	83.33	83.33	50	99	66.67	100
Repeatability (%)	94.83	96.12	94.45	95.96	87.06	99.44	96	98.4

Figures

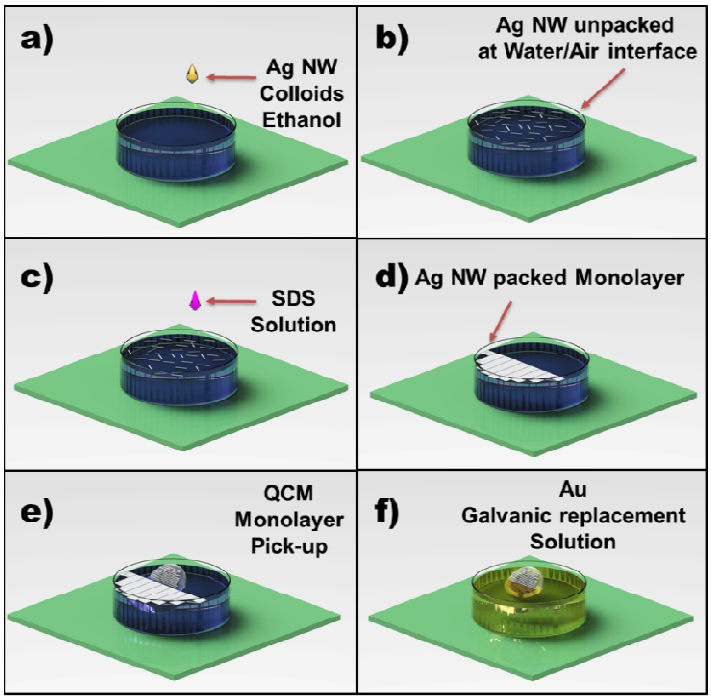

Figure 1

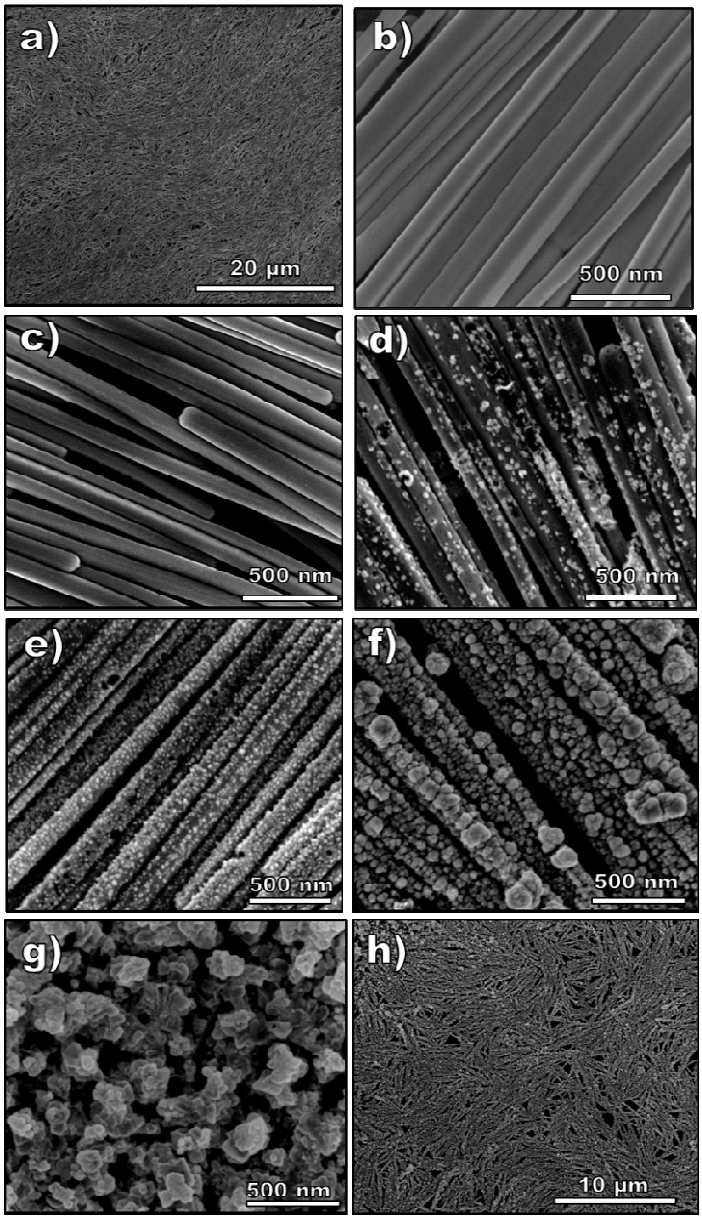

Figure 2

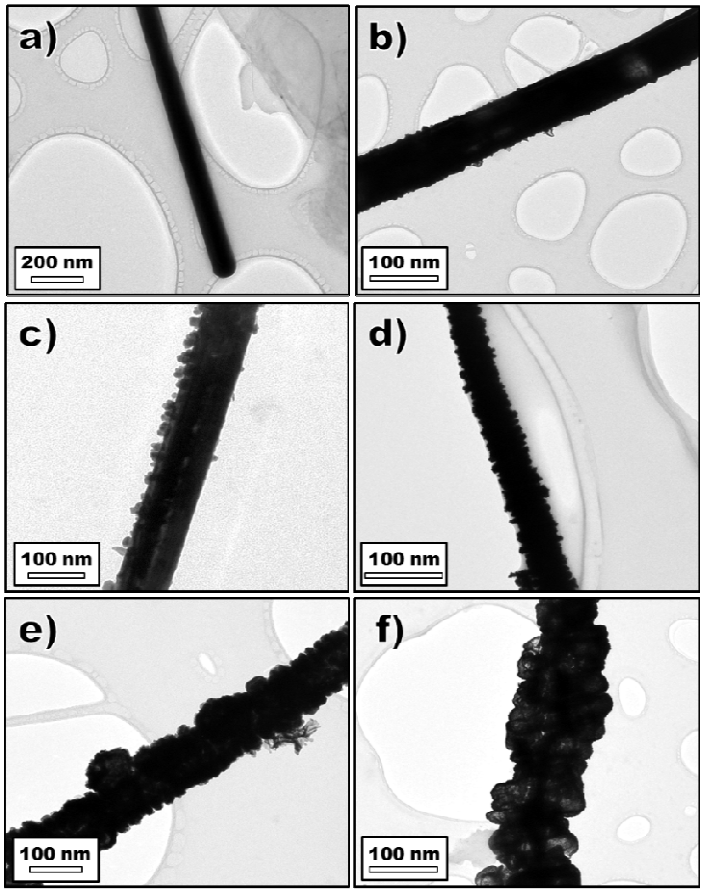

Figure 3

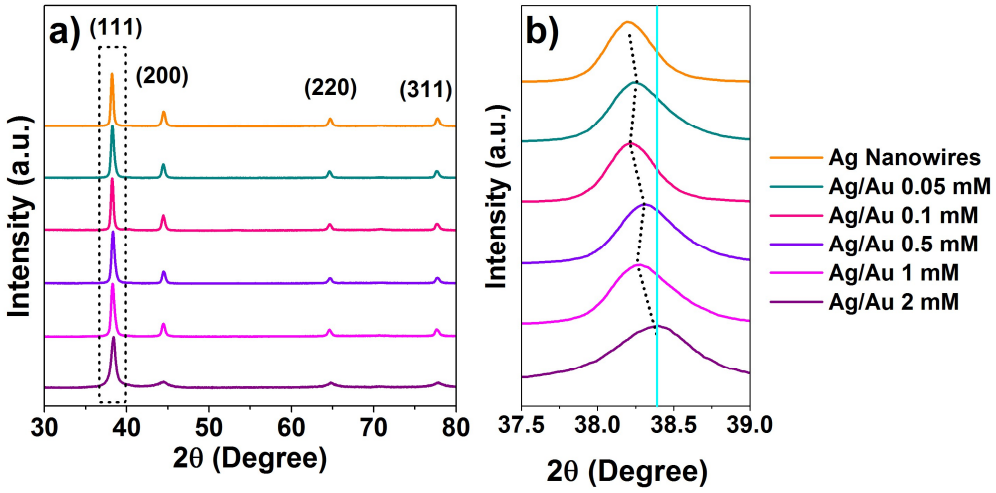

Figure 4

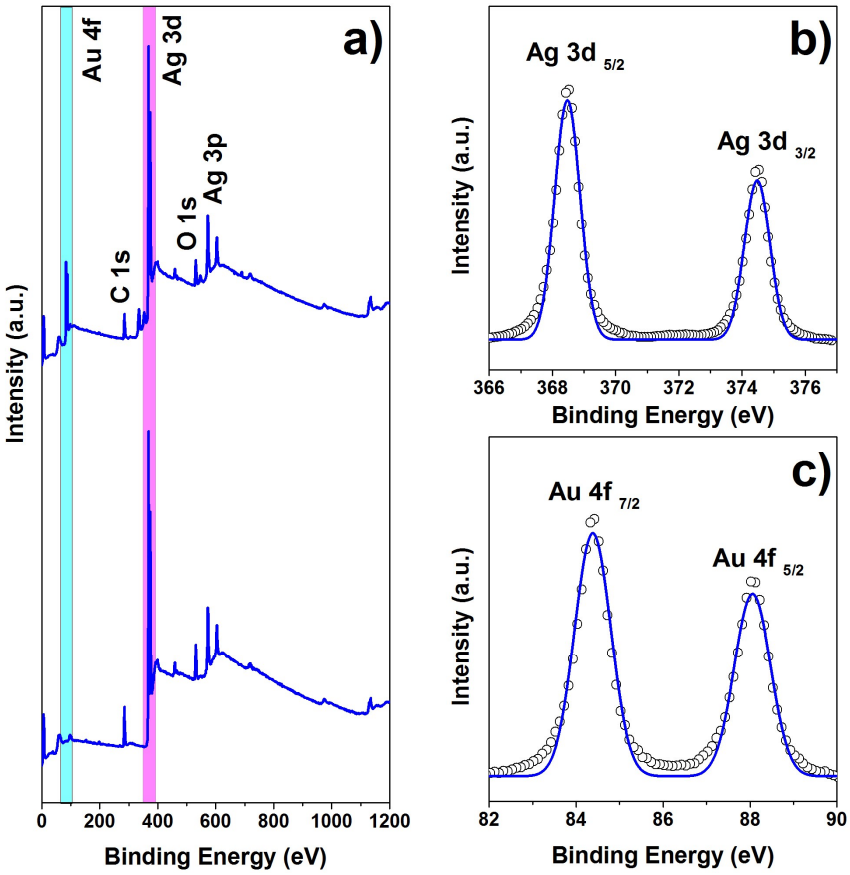

Figure 5

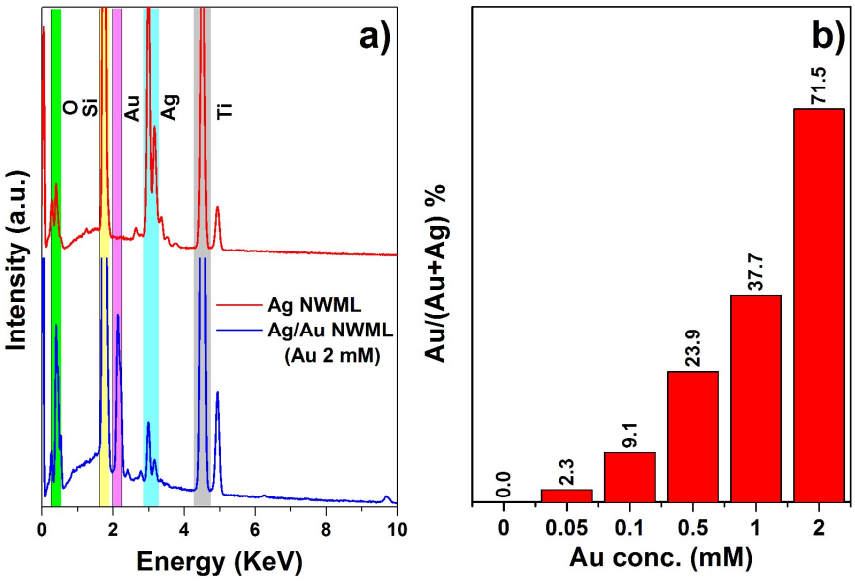

Figure 6

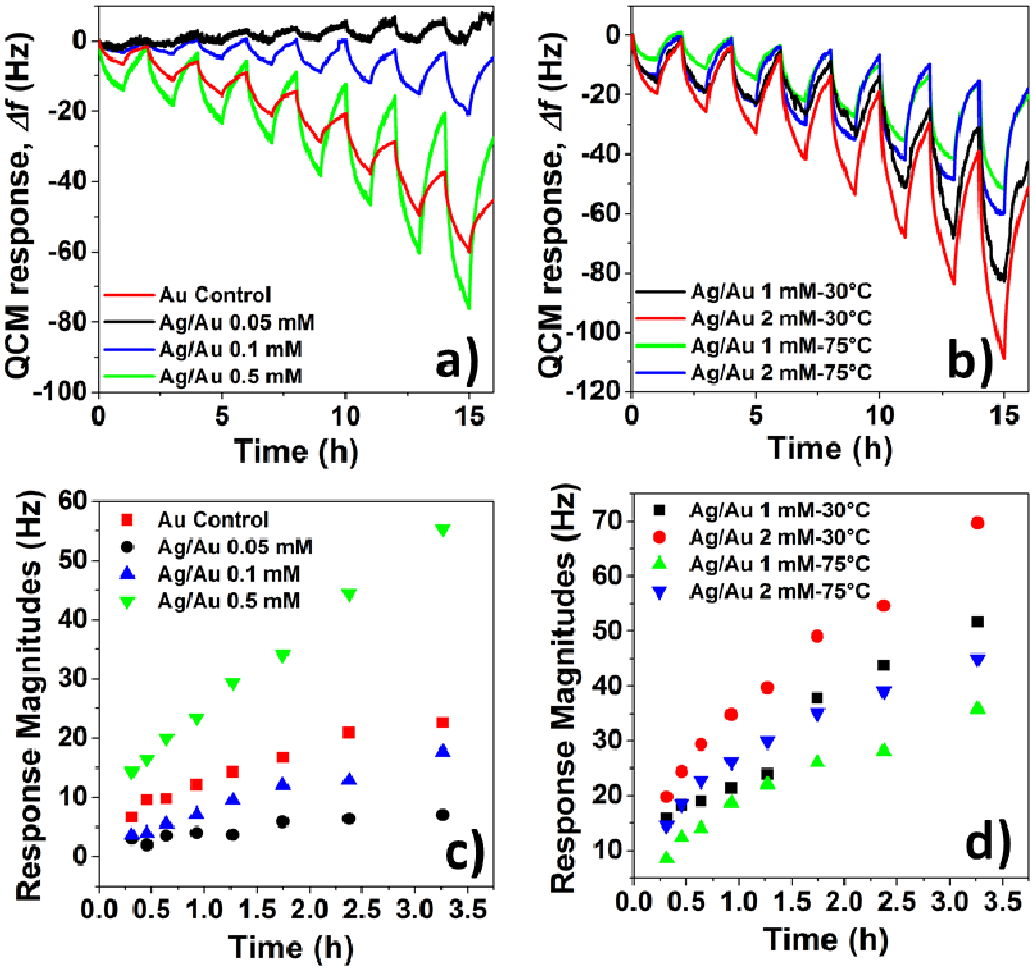

Figure 7

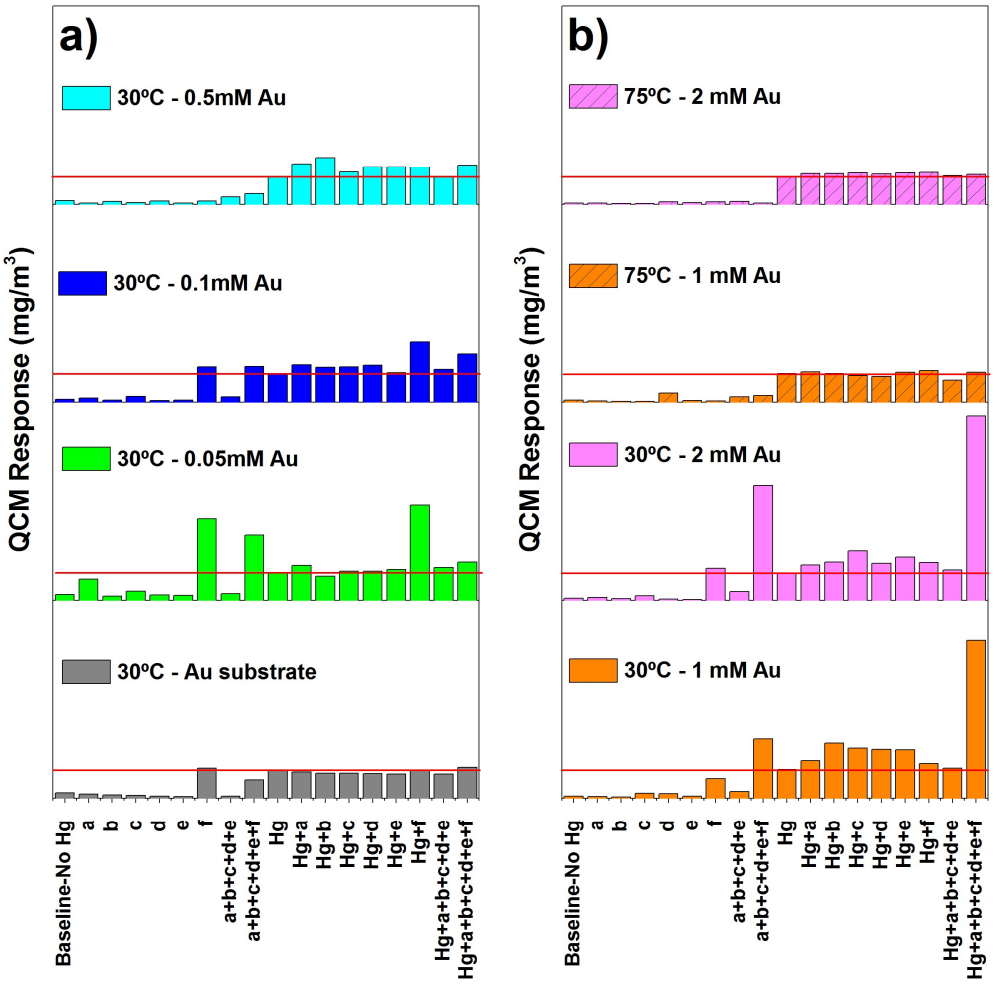

Figure 8